International Journal of Heat and Mass Transfer 52 (2009) 574–581

Contents lists available at ScienceDirect

International Journal of Heat and Mass Transfer

journal homepage: www.elsevier.com/locate/ijhmt

Biofilm affected characteristics of porous structures

Maryam Shafahi, Kambiz Vafai *

Department of Mechanical Engineering, University of California, A363 Bourns Hall, 92521-0425 Riverside, CA, USA

ARTICLE INFO

Article history:
Received 30 April 2008
Received in revised form 11 July 2008
Available online 9 September 2008

Keywords:
Biofilm
Porous media
Permeability
Porosity

ABSTRACT

Formation of biofilm within a porous matrix reduces the pore size and the total open space of the system, altering the porosity and permeability of the medium. This change in the pore size distribution can be quantified by expressing the porous structure with a proper geometrical model. A set of pertinent multispecies biofilm models is used to arrive at the dynamic biofilm thickness distribution. The obtained results are utilized within a modified Kozeny–Carman framework to establish permeability and porosity distribution during the biofilm formation. The biofilm thickness and the obtained permeability profile for a special microorganism, *Pseudomonas aeruginosa*, are compared with available experimental data. The potential reasons attributing to the differences between the numerical and experimental data are discussed.

© 2008 Elsevier Ltd. All rights reserved.

1. Introduction

Biofilm can form in various environments on the condition that a surface, nutrients and water are accessible. Studies show that the principal mode of microbial existence in most natural and synthetic environments is related to surface associated biofilms [1]. As such they are found in natural habitats like rivers and streams, on the surface of plants, on teeth and oral epithelium and on the mucosa of the digestive tract. Biofilm also exists in metal working systems, the ship hulls and oil exploration platforms [2].

Biofilms can be useful or harmful depending on their area of existence. They are quite helpful in bioremediation, microbial enhanced oil recovery and metal extraction; yet they can be damaging in water pipes, heat exchangers, submarines and human bodies. They are able to act as a barrier against antimicrobial compounds, control interfacial processes, harbor pathogenic microorganisms, consume pollutants and ease genetic material transport [3]. Recently it has been noted that biofilms are engaged in about 65% of all human diseases [4]. In mining industry, methods are developing for microbial enhanced leaching of metals from ores and recovery of metals from solutions. Subsurface biofilms also offer the potential for biotransformation of organic compounds; so they could be used for treating contaminated groundwater supplies [5].

Investigating the biofilm spatial distribution and composition of microorganisms is necessary to understand different functions of biofilms in different scenarios. Amongst different approaches to study the biofilms, modeling is a necessary tool constituting the most pertinent aspect of research in this area [6]. Modeling enables researchers to express and examine their hypotheses and analyze the obtained experimental data.

Generally, there are two different approaches used in modeling the biofilms. A more prevalent approach is to assume the biofilm as a continuous layer. Another approach is based on considering it as patchy aggregates that accumulate in pore throats. Some studies show that biofilms are continuous for normalized surface loadings greater than one, but appear to become discontinuous for values less than about 0.25. For cases with sufficient nutrients, continuous layer assumption better matches with reality. For the low-load cases, it is important to distinguish between the continuous and discontinuous biofilms in order to have a more precise prediction for spatial distribution and permeability reduction [7]. It could be assumed that a biofilm is composed of two different parts, i.e., base and surface films. The base film components are packed and rather continuous, while the surface film medium is more discontinuous [8]. One of the very common discrete-stochastic methods used in this field is Cellular Automata (CA), in which nutrient and biomass are characterized by individual particles [9]. In this approach, the biofilm is represented as a continuous layer and its properties primarily change in a direction normal to the solid surface.

A number of investigations have been performed on estimating the steady state thickness of biofilm [10–15]. In some of these works [10,13,14], it is assumed that there is a minimum substrate concentration that can support steady state thickness of biofilm and below that certain amount; no steady state biofilm activity exists. Biofilm includes different phases such as liquid and solid. Wanner and Gujer [16] developed a multicomponent but homogeneous model to predict biofilm growth. Later, they expanded their model [8] to consider liquid and solid phases within the biofilm.

* Corresponding author.
E-mail address: Vafai@engr.ucr.edu (K. Vafai).

0017-9310/$ - see front matter © 2008 Elsevier Ltd. All rights reserved.
doi:10.1016/j.ijheatmasstransfer.2008.07.013

Nomenclature

C	concentration
d	sphere diameter
D	diffusion coefficient
k	reaction rate constant for inactivation
K	absolute permeability
L	biofilm thickness
q	number of contacts within a unit cell
M	specific surface
r	reaction term
u	velocity
V	bulk volume of a unit cell
Y	biomass yield coefficient

Greek symbols

α	arrangement packing factor
ε	porosity
η	viscosity
λ	biomass detachment coefficient
μ	specific growth rate
$\overline{\mu}$	mean specific growth rate
$\hat{\mu}$	maximum specific growth rate
ξ	normalized coordinates
ρ	density
σ	biomass exchange velocity between biofilm and bulk liquid

Subscripts

b	biofilm
i	microbial index
j	nutrient index
m	microbial phase
n	nutrient phase
l	liquid phase

That model was modified to include the solid (particulate) phase diffusive flux and the liquid (dissolved) phase advective flux. A summary of the pertinent biofilm models studied in this work is given in Table 1.

In this work, a set of biofilm models is utilized based on three main processes that occur inside a film: consumption of nutrients, nutrient transport and volume expansion of biomass. Our results are compared with the available pertinent literature.

Biofilm growth in a porous medium and the subsequent reduction in permeability are important in a number of applications such as water treatment, enhanced oil recovery, groundwater recharge and in situ bioremediation. The rate of biotransformation is directly affected by the porous medium characteristics such as permeability and pore velocity distribution [5]. As such, biofilm control in porous media provides significant opportunities to improve the performance of industrial and environmental processes utilizing prescribed biofilm growth and distribution. An efficient use of this phenomenon by engineers requires an understanding of the relationship between the hydrodynamic properties of porous medium and the temporal and spatial distribution of the biofilm. In some of the formulations biofilm is considered as a porous medium [8,17] and its properties are investigated at the micro-scale level while in other models, flow in the external medium is coupled with the biofilm equations [18,19] and the macro-scale picture is also brought into the model.

Several studies have been focused on the critical role of a continuous biofilm growth on the porous matrix. Although it is generally understood that biofilm formation can reduce the permeability of a medium, different explanations exist on how this reduction happens. Investigations have been done on a wide variety of porous media, including core samples from fields as well as synthetic media (e.g., glass spheres). A large decline in permeability (65–95%) has been observed for most cases as a result of biofilm growth [5]. One of the earliest works in this area has been performed by Allison [20] who observed significant reductions in the hydraulic conductivity of saturated porous media caused by microorganisms. Some studies [21–23,5] support the concept of a continuous biofilm on a surface such as that of grains. This approach was quantified and incorporated into a transport model that achieved realistic explanations of experi-

Table 1
Summary of pertinent biofilm models

Generalized governing equation $\frac{\partial \mathbf{D}}{\partial t} + \nabla \cdot \mathbf{j} = \mathbf{R}$

$$\mathbf{D} = \begin{bmatrix} D_1 \\ D_2 \\ D_3 \end{bmatrix} = \begin{bmatrix} \rho_m \varepsilon_m \\ \varepsilon_l C_n \\ \varepsilon_l \end{bmatrix} = \begin{bmatrix} \textit{Microbial phase concentration} \\ \textit{Nutrient phase concentration} \\ \textit{Liquid phase porosity} \end{bmatrix}$$

$$\mathbf{j} = \begin{bmatrix} j_{11} + j_{12} \\ j_{21} + j_{22} + j_{23} \\ j_{31} + j_{32} \end{bmatrix} = \begin{bmatrix} \varepsilon_m \rho_m u - D_m \nabla(\varepsilon_m \rho_m) \\ -(1-\varepsilon_1) u C_n - \varepsilon_1 D_n \nabla C_n + \sum_{m=1}^{N_m} \frac{D_m}{\rho_m} \nabla(\varepsilon_m \rho_m) C_n \\ u\varepsilon_l + \sum_{m=1}^{N_m} \frac{D_m}{\rho_m} \nabla(\varepsilon_m \rho_m) \end{bmatrix}$$

Monod: $\mu = \mu_{\max} \frac{\rho}{K_s + \rho}$ Double Monod: $\mu = \mu_{\max} \frac{\rho_1}{K_{s1} + \rho_1} \frac{\rho_2}{K_{s2} + \rho_2}$

References	**D** (array of variables)	**j** (flux)	**R** (reaction terms)	ε_l (liquid porosity)
Wanner and Gujer [16]	$\begin{bmatrix} D_1 \\ D_2 \end{bmatrix}$	$\begin{bmatrix} j_{11} \\ j_{22} \end{bmatrix}$	Double Monod	–
[8,17,34,36,37]	$\begin{bmatrix} D_1 \\ D_2 \end{bmatrix}$	$\begin{bmatrix} j_{11} \\ j_{21} + j_{22} \end{bmatrix}$	Double Monod	constant & variable
Wanner et al. [35]	$\begin{bmatrix} D_1 \\ D_2 \\ D_3 \end{bmatrix}$	$\begin{bmatrix} j_{11} + j_{12} \\ j_{21} + j_{22} + j_{23} \\ j_{31} + j_{32} \end{bmatrix}$	Double Monod	variable
Rittman and McCarty [10]	–	$[j_{22}]$	Monod	–
Rittmann and Manem [14]	–	$\begin{bmatrix} j_{11} \\ j_{22} \end{bmatrix}$	Monod	–

mental data carried out in columns packed with spheres having 0.12–1 mm diameters [18].

The other key factor in biofilm formation process is the type of microorganism. Several experimental studies have been done on the biofilm performance with different microbes.

One of the most common bacteria utilized in biofilm studies is *Pseudomonas aeruginosa* (Pa) which has been investigated under high substrate loading [17], competitive [1], unsteady [5], and steady state conditions [24]. This species seems to produce a monolayer of cells on the solid surface when others form segregated colonies [25]. It should be noted that Pa is a major cause of cystic fibrosis [28].

In Bakke et al.'s work [24] nutrient removal rate vs. specific growth rate is investigated. Their data matches well with a steady state mathematical model they had introduced for biofilm formation. In Stewart et al.'s work [1] competition between Pa and *Klebsiella pneumonia* is studied. The spatial distribution for different microorganisms is examined by fluorescent labeling. In these works biofilm thickness was not established. As such, our results are compared with two sets of experimental data given in Cunningham et al. [5] and Wanner et al.'s work [17].

The purpose of this work is to assess the porosity and permeability alterations in a porous medium during the biofilm formation. First, a set of multispecies biofilm models will be analyzed. Different physical attributes that affect the biofilm thickness will be investigated for one of these representative models. Next, the dynamic biofilm thickness is applied to a porous network, which is made of spheres with equal and non-equal diameters. Biofilm affected permeability and porosity temporal distributions are obtained from the described biofilm models. Finally, the presented models are examined for a certain type of bacteria, *Pseudomonas aeruginosa*, and numerical and experimental data are compared.

2. Governing equations

2.1. Microbial phase

Conservation of mass for microbes can be presented by

$$\frac{\partial \rho_i}{\partial t} + \nabla \cdot j_i^m = r_i, \quad i = 1, \ldots, N_m \tag{1}$$

Let $\rho = \rho(t,x)$ denote the density of microbial species at time t and position x. Assuming that the bulk motion is dominant, the flux can be presented as

$$j_i^m = \rho_i u \tag{2}$$

Assuming that microbial species are incompressible and $\varepsilon = \varepsilon(t,x)$ is the volume fraction of species

$$\rho_i(t,x) = \varepsilon_i \rho_i^* \quad \forall x \in [0,L], \ t \geqslant 0 \tag{3}$$

where ρ_i^* is taken constant for each microbe. Using Eqs. (2) and (3) in Eq. (1) results in

$$\frac{\partial \varepsilon_i}{\partial t} + \nabla \cdot (u\varepsilon_i) = \frac{1}{\rho_i^*} r_i(C_j, \varepsilon_i), \quad i = 1, \ldots, N_m \tag{4}$$

where C_j is the nutrient concentration. The reaction term r_i and the average net growth rate $\bar{\mu}$ are expressed as:

$$r_i = \mu_i \rho_i \Rightarrow \bar{\mu} = \sum_{i=1}^{N_m} \mu_i \varepsilon_i \tag{5}$$

where μ_i is the net growth rate for a microbial species. Combining Eqs. (4) and (5) results in

$$\frac{\partial \varepsilon_i}{\partial t} = [\mu_i - \bar{\mu}]\varepsilon_i - u \cdot (\nabla \varepsilon_i) \tag{6}$$

2.2. Nutrient phase

Conservation of mass for nutrients, considering the diffusive flux, can be represented by

$$\frac{\partial C_j}{\partial t} = r_j + \nabla \cdot (D_j \nabla C_j), \quad j = 1, \ldots, N_n \tag{7}$$

3. Microbial and nutrient set of equations

The total set of governing equations for the transport of microbes and nutrients can be presented as:

$$\begin{cases} \dfrac{\partial \mathbf{D}}{\partial t} + \nabla \bullet \mathbf{j} = \mathbf{R} \\ \mathbf{D} = \begin{bmatrix} \varepsilon_m \\ \varepsilon_l C_n \\ \varepsilon_l \end{bmatrix} \\ \mathbf{j} = \begin{bmatrix} \varepsilon_m u \\ u C_n - D_n \nabla C_n \\ u \varepsilon_l \end{bmatrix} \\ \mathbf{R} = \begin{bmatrix} (\mu_i - \bar{\mu})\varepsilon_i \\ r_j \\ 0 \end{bmatrix} \end{cases} \tag{8}$$

3.1. Models I–IV

Based on the set of governing equations for microbial activities, four pertinent models are chosen. It is assumed in model I that microbial species occupy the entire space of biofilm while in models II–IV, liquid and solid phases exist within the film. Microbes and their products constitute the solid or particulate phase and nutrients or dissolved components exist in liquid phase inside the film. Model II includes the advective flux of particulate phase and diffusive flux of dissolved phase with the constant initial liquid porosity. These models enable us to assess the effect of physical attributes of the presence or absence of pertinent terms. Model III has the physical attributes of model II plus an advective flux for the dissolved phase. Model IV's difference with model II is the inclusion of temporal liquid phase porosity. The sensitivity of the results with respect to a change in initial values of biofilm thickness and liquid porosity is also examined for the case of Pa. Table 2 summarizes the governing equations representing these biofilm models that are being investigated in this work. It should be noted that models I to IV capture the essential element and physical attributes of the models in Table 1.

Table 2
Summary of models I, II, III and IV

Generalized governing equation:	$\frac{\partial \mathbf{D}}{\partial t} + \nabla \cdot \mathbf{j} = \mathbf{R}$		
Models	**D**	**j**	**R**
Model I	$\begin{bmatrix} \varepsilon_m \\ C_n \end{bmatrix}$	$\begin{bmatrix} \varepsilon_m u \\ -D\nabla C_n \end{bmatrix}$	Double Monod
Model II	$\begin{bmatrix} \varepsilon_m \\ \varepsilon_l C_n \end{bmatrix}$	$\begin{bmatrix} \varepsilon_m u \\ -D\nabla C_n \end{bmatrix}$	Double Monod
Model III	$\begin{bmatrix} \varepsilon_m \\ \varepsilon_l C_n \end{bmatrix}$	$\begin{bmatrix} \varepsilon_m u \\ uC_n - D_n \nabla C_n \end{bmatrix}$	Double Monod
Model IV	$\begin{bmatrix} \varepsilon_m \\ \varepsilon_l C_n \\ \varepsilon_l \end{bmatrix}$	$\begin{bmatrix} \varepsilon_m u \\ uC_n - D_n \nabla C_n \\ u\varepsilon_l \end{bmatrix}$	Double Monod

3.2. ξ coordinate

It should be noted that at $x = 0$ and $x = L$ (film interface with the bulk fluid) the function $\varepsilon_i = \varepsilon_i(t,x)$ which shows the spatial distribution of the microorganisms, is discontinuous. When the film grows or shrinks, the discontinuity at $x = L$ moves in space. To operate within a fixed domain, a transformation from (x,t) to $(\xi(x,t),t)$ is introduced, where

$$\xi(x,t) = \frac{x}{L(t)} \tag{9}$$

Along with the following boundary conditions

$$\left.\frac{\partial \varepsilon_i}{\partial \xi}\right|_{\xi=0} = 0 \tag{10}$$

$$\left.\frac{\partial C_j}{\partial \xi}\right|_{\xi=0} = 0 \tag{11}$$

$$C_j|_{\xi=1} = C_{j,bulk} \tag{12}$$

3.3. Mass boundary layer

As the source of nutrient in most biofilm systems is inside the bulk fluid, biofilm activities are dependent on the transport of nutrients through the interface of the biofilm and the bulk fluid. The nutrient mass transfer into the biofilm is driven by the concentration gradient of nutrient across the boundary layer. The nutrient flux perpendicular to the biofilm surface is:

$$j_n = h_m(C_{n,bulk} - C_{n,interface}) \tag{13}$$

where h_m is the mass transfer coefficient, $C_{n,bulk}$ is the nutrient concentration in the bulk fluid and $C_{n,interface}$ is the nutrient concentration at the interface. Our simulation results show that the mass transfer resistance in the biofilm boundary layer is extremely low and Eq. (12), complete mixing, is an adequate condition in our analysis. It should be noted that the initial thickness of the biofilm and distribution of nutrients and microbes are required to solve each set of governing equations representing a given model.

4. Reaction terms and physical attributes

In this work, a mixture of microbes and nutrients are considered. Specifically, two microbes and three nutrients are analyzed. Microbial species are assumed to be Heterotroph and Autotroph and nutrients are organic Carbon, Ammonium and dissolved Oxygen. A double Monod expression is used for the reaction terms. The net growth rates of microbial species are:

$$\mu_1 = \hat{\mu}_1 \frac{C_3}{K_{o1}+C_3}\frac{C_1}{K_{s1}+C_1} - b_1\frac{C_3}{K_{o1}+C_3} - k_1 \quad \text{(Heterotrophic)} \tag{14}$$

$$\mu_2 = \hat{\mu}_2 \frac{C_3}{K_{o2}+C_3}\frac{C_2}{K_{s2}+C_2} - b_2\frac{C_3}{K_{o2}+C_3} - k_2 \quad \text{(Autotrophic)} \tag{15}$$

Rate of conversion for nutrients can be specified as:

$$r_1 = -\frac{1}{Y_1}\left(\hat{\mu}_1\rho_1^*\varepsilon_1\frac{C_3}{K_{o1}+C_3}\frac{C_1}{K_{s1}+C_1}\right) \tag{16}$$

$$r_2 = -\frac{1}{Y_2}\left(\hat{\mu}_2\rho_2^*\varepsilon_2\frac{C_3}{K_{o2}+C_3}\frac{C_2}{K_{s2}+C_2}\right) \tag{17}$$

$$r_3 = -\frac{\alpha_1 - Y_1}{Y_1}\left(\hat{\mu}_1\rho_1^*\varepsilon_1\frac{C_3}{K_{o1}+C_3}\frac{C_1}{K_{s1}+C_1}\right) - b_1\rho_1^*\varepsilon_1\frac{C_3}{K_{o1}+C_3} - \left(\frac{\alpha_2 - Y_2}{Y_2}\right)\hat{\mu}_2\rho_2^*\varepsilon_2\frac{C_3}{K_{o2}+C_3}\frac{C_2}{K_{s2}+C_2} - b_2\rho_2^*\varepsilon_2\frac{C_3}{K_{o2}+C_3} \tag{18}$$

The biofilm expansion velocity is

$$u = L\int_0^{\xi}\bar{\mu}\,d\xi \tag{19}$$

where $\hat{\mu}_1$, $\hat{\mu}_2$, K_{o1}, K_{o2}, K_{s1}, K_{s2}, k_1, k_2, b_1, b_2, Y_1, Y_2 are empirically determined constants taken from Wanner and Gujer [16]. In Eqs. (14)–(18), C_1, C_2, C_3 designate the concentration of nutrients (organic Carbon, Ammonium and dissolved Oxygen, respectively).

Utilizing upwind differencing, the set of equations given in (8) are discretized. Nutrient concentrations are solved implicitly and using these newly obtained concentrations; equations for microbial species and biofilm thickness are updated. In what follows results from model I compared with those obtained by Wanner and Gujer [16]. The physical cases considered in this work are:

Case 1 – unrestricted growth of biofilm
In this case it is assumed that there is no biofilm detachment and nutrient concentrations in the bulk fluid remain constant. Under these conditions the thickness of the biofilm increases without restriction as can be seen in Fig. 1, the current results match very well with those by Wanner and Gujer [16] under several different conditions.

Case 2 – change in nutrient concentrations of bulk fluid
This case illustrates the effect of a sudden change in the nutrient concentrations in the bulk fluid on the biofilm growth. As seen in Fig. 1, a sudden cut off of one of the nutrients after 6 days shows that at first the rate decreases substantially, but after a while the other type of microbes which are not dependent on the removed nutrient supply the biofilm growth and as such compensate the cutting effect.

Case 3 – biofilm growth under shear stress
Compared with case 1, this case includes a continuous loss of biomass due to shear stress. The loss of microorganisms is continuous and proportional to their respective species concentration at the interface of the biofilm (film–bulk interface). To account for this shear stress the interface velocity is modified by introduction of a damping factor σ as utilized in the work of Wanner and Gujer [16]. This modified interface velocity can be represented by

$$u|_{\xi=1} = L\int_0^1\bar{\mu}\,d\xi + \sigma \tag{20}$$

$$\sigma = -\lambda L^2 \tag{21}$$

The parameter σ is assumed to be proportional to L^2. As seen in Fig. 1, for this case, due to shear, biofilm growth is substantially decreased and may even temporarily become negative during rapid population shifts. However after the passage of some time, as expected, the biofilm reaches a steady state value.

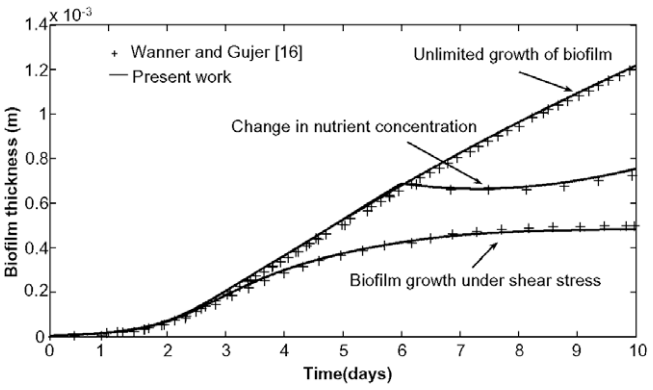

Fig. 1. Comparison of biofilm thicknesses for model I various cases with Wanner and Gujer [16].

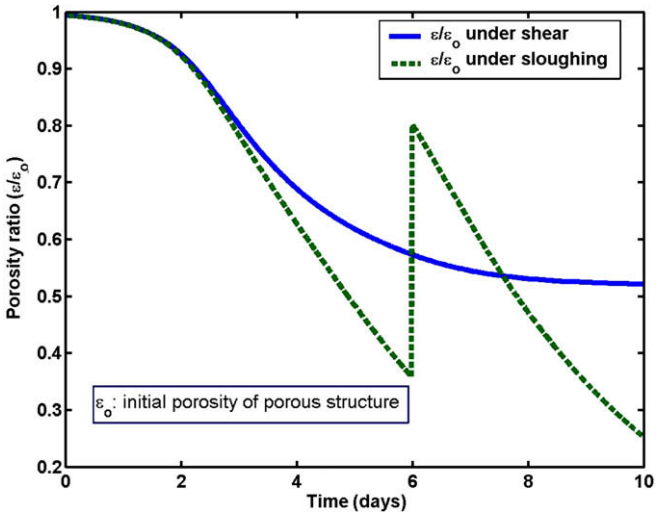

Fig. 2. Porosity ratio temporal distribution for biofilm growth under shear and sloughing (starting on the 6th day).

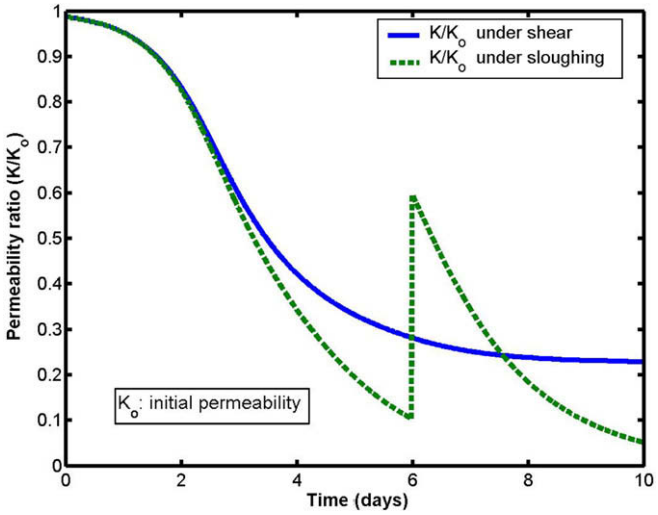

Fig. 3. Permebility ratio temporal distribution for biofilm growth under shear and sloughing (starting on the 6th day).

Case 4 – biomass growth under sloughing
When critical conditions are reached, considerable portions of biomass are assumed to suddenly slough off the film. This case attempts to simulate the physical attributes of sloughing on the 6th day. Figs. 2 and 3 display typical characteristics of sloughing for a case where critical conditions are assumed to be reached at a certain point in time.

5. Geometrical model representation of a porous medium

In order to investigate the effect of biofilm formation the capillary tube model is first adapted to represent the porous structure. The starting point in capillary tube models is the Hagen–Poisseule's relationship for the steady flow through a single straight circular capillary tube in the flow direction. Utilizing Darcy's law and average velocity from the capillary tube model, an established relationship for permeability based on porous medium characteristics was established by Kozeny [26] which was later modified by Carman [27] as:

$$K = c_0 \frac{\varepsilon^3}{M^2} \tag{22}$$

where the specific surface, M, is:

$$M = \frac{A}{V_{bulk}} \tag{23}$$

where, A is interstitial surface area. Eq. (22) is called Kozeny equation and can be used to estimate the spherical network permeability as well. In the spherical case, the empty spaces among the spheres are the capillary tubes with non-circular cross-sections [29].

5.1. Homogenous porous matrix

Consider a network of spheres with equal diameters representing the porous structure. For such a porous matrix representation, the bulk volume of the unit cell occupied by a sphere and subsequently its porosity and specific surface can be represented as [30–33]

$$V = \alpha\, d^3 \tag{24}$$

$$\varepsilon = \frac{V - V_{sphere}}{V} = 1 - \left(\frac{\pi}{6\alpha}\right) \tag{25}$$

$$M = \frac{A}{V_{bulk}} = \frac{\pi d^2}{\alpha d^3} = \frac{\pi}{\alpha d} \tag{26}$$

where α and d are the arrangement packing factor and the sphere diameter, respectively.

5.2. Non-homogeneous porous matrix

In order to characterize a non-homogenous porous structure; a network of spheres with different diameters can be considered. If a cubic arrangement of spheres of diameter d includes a sphere of diameter d' in the center, porosity and specific surface are given as [22]:

$$d' = (\sqrt{3} - 1)d \tag{27}$$

$$\varepsilon = 1 - \frac{\pi}{6}\left[1 + (\sqrt{3} - 1)^3\right] \tag{28}$$

$$M = \frac{\pi}{d}\left(5 - 2\sqrt{3}\right) \tag{29}$$

6. Biofilm growth

The discussed biofilm models are applied to the presented network of spheres with equal and non-equal diameters. As the biofilm thickness increases the volume of spheres increases and the available interpore cross-sectional area decreases. The volume of a coated sphere without any contact point can be specified as:

$$V_b = \frac{4\pi}{3}\left(\frac{d}{2} + L\right)^3 \tag{30}$$

where, L is the biofilm thickness forming over the sphere surface. Each sphere can have q contact points with the adjacent ones. This is taken into account by deducting the volumes of q contact locations from the total coated sphere volume.

$$V_b^s = \frac{4\pi}{3}\left(\frac{d}{2} + L\right)^3 - q\left\{\pi\left(\frac{2}{3}L^3 + L^2\left(\frac{d}{2}\right)\right)\right\} \tag{31}$$

The bulk volume of a unit cell occupied by a sphere is given by Eq. (24). For a unit cell configuration made up of one sphere in contact with q other spheres, the porosity and the specific surface area can be prescribed as [22]:

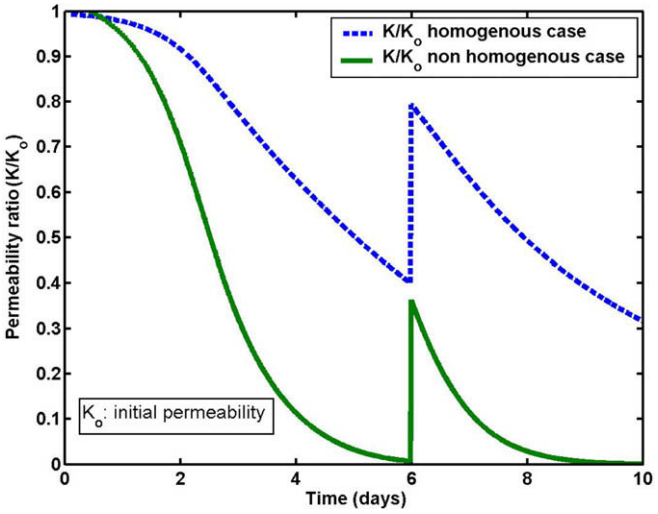

Fig. 4. Permeability ratio temporal distribution for homogenous and non-homogenous porous matrix under sloughing conditions (starting on the 6th day).

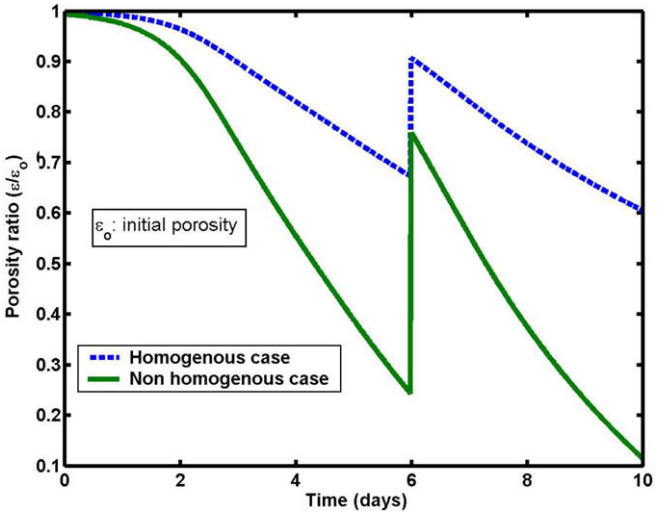

Fig. 5. Porosity ratio temporal distribution for homogenous and non-homogenous porous matrix under sloughing conditions (starting on the 6th day).

$$\varepsilon_b = 1 - \frac{V_b^s}{V} = 1 - \frac{\pi}{\alpha}\left(\frac{1}{6} + \frac{L}{d} + \left(2 - \frac{q}{2}\right)\left(\frac{L}{d}\right)^2 + \left(\frac{4}{3} - \frac{2q}{3}\right)\left(\frac{L}{d}\right)^3\right) \tag{32}$$

$$M_b = \frac{\pi}{\alpha d}\left[\frac{(2-q)}{2}\left(\frac{2L}{d}\right)^2 + \frac{(4-q)}{2}\left(\frac{2L}{d}\right) + 1\right] \tag{33}$$

For the non-homogenous case the biofilm affected porosity and permeability are presented as follows [22]:

$$\varepsilon_b = 1 - \pi\left[\hat{a}\left(\frac{2L}{d}\right)^3 + \hat{b}\left(\frac{2L}{d}\right)^2 + \hat{c}\left(\frac{2L}{d}\right) + \hat{d}\right] \tag{34}$$

$$M_b = \frac{\pi}{d}\left[\hat{e}\left(\frac{2L}{d}\right)^2 + \hat{f}\left(\frac{2L}{d}\right) + \hat{g}\right] \tag{35}$$

where $\hat{a}, \hat{b}, \hat{c}, \hat{d}, \hat{e}, \hat{f}, \hat{g}$ are known constants. The biofilm affected permeability K_b is found by using ε_b and M_b in the Kozeny–Carman relationship assuming the same c_0 as in the original equation [22]

$$K_b = c_0 \frac{\varepsilon_b^3}{M_b^2} \tag{36}$$

After obtaining the transient biofilm growth, the transient permeability and porosity distributions can be obtained from Eqs. (36), (34) and (32). Effects of shear stress and sloughing on the permeability and porosity distribution are shown in Figs. 2 and 3. In Figs. 4 and 5 the permeability profiles for biofilm formation over homogenous and non-homogenous porous structures are compared. As seen in these figures, porosity and permeability reduction rates are more pronounced for the non-homogenous case. The non-homogenous model is a better presentation of a natural porous medium, such as soil. However, in our comparisons with experimental data for homogenous packed bed reactor the homogenous model is utilized.

7. Comparison with experimental data

The results from the models presented in this work are compared with the experimental data presented by Cunningham et al. [5] and Wanner et al. [17] utilizing the Monod parameters given in the latter work. It is assumed that biofilm forms over spheres with diameters of 1 mm with a common microorganism namely, *Pseudomonas aeruginosa*. Glucose is chosen as the limiting nutrient. Comparisons with experimental results for biofilm thickness are shown in Figs. 6–8. As seen in Fig. 6, model I overpredicts the thickness of biofilm for later times. Models II, III and IV under predict the experimental data of Cunningham et al. [5] for earlier times while over predicting both set of experimental data for later times. Biofilm thickness in all models, presented in Fig. 6, is almost zero for the earlier times, which matches the data of Cunningham et al. [5]. Model I is based on the assumption that microbes occupy the entire biofilm space. However, models II, III and IV treat water and microbial phases separately. These models may be considered to be a closer representation of the real case where the biofilm itself is characterized as a porous medium consisting of particulate or microbial phase as well as the dissolved nutrients, which are within the liquid phase.

The sensitivity of the results with respect to initial liquid porosity and biofilm thickness are shown in Figs. 7 and 8. As seen in these figures, biofilm thickness changes with different initial conditions are significant during the transient phase. It can be seen that while the effect of different initial thicknesses during the transient phase is significant; at steady state the differences are substantially diminished. Further, we had established that there is not much difference when adding nutrient's advective flux (model III) or taking the effect of liquid porosity change vs time into

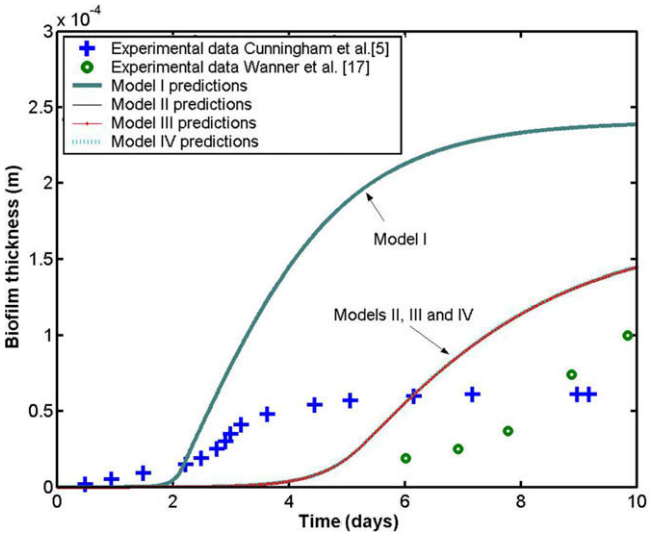

Fig. 6. Comparison of models' biofilm thicknesses with experimental data.

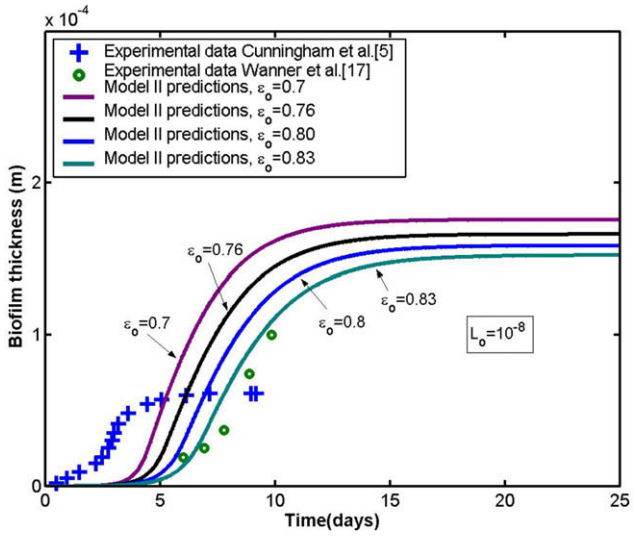

Fig. 7. Comparison of model II predictions and experimental data for biofilm thicknesses starting with different initial liquid porosities within the film.

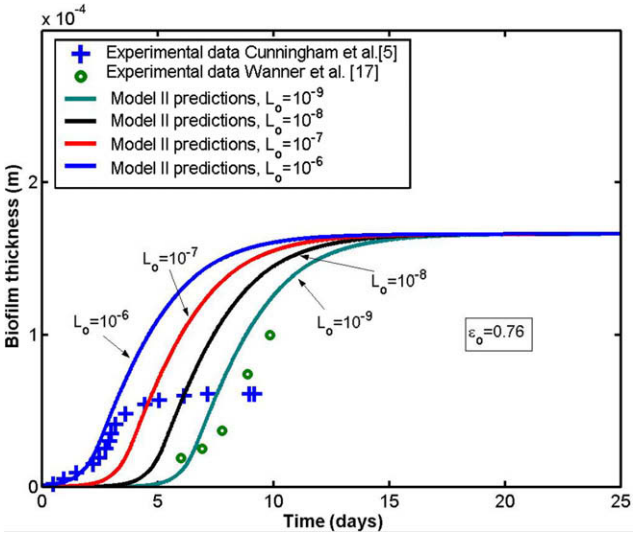

Fig. 8. Comparison of model II predictions and experimental data for biofilm thicknesses starting with different initial thicknesses of the film.

account (model IV). However, the effect of different initial liquid porosities is significant both at steady state as well as the transient phase. These biofilm models are based on an unlimited growth space for the biomass. When applying the models to a porous medium, there is a limitation for available growth space. As such the growth of biofilm is continued only until such time when it encounters the next solid boundary. The obtained biofilm thicknesses from these two models are compared with two different sets of experimental data presented by Cunningham et al. [5] and Wanner et al. [17]. It should be noted that the models predictions qualitatively match better with the experimental results of Cunningham et al. [5]. The sphere network model described earlier in this work is applied along with dynamic thickness of biofilm to obtain the porosity and permeability of the medium during the biofilm formation. Numerical results for permeability are compared with experimental data of Cunningham et al. [5] in Fig. 9. The delayed formation of the biofilm as seen in Fig. 6, compared to the experimental results, impacts the temporal permeability prediction curves. As seen in Fig. 9, due to a late biofilm formation for Models II, III and IV the permeability profile displays a delayed

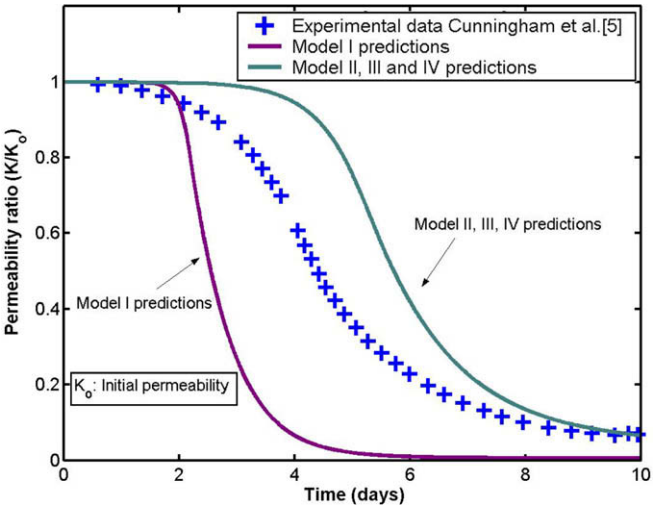

Fig. 9. Comparison of temporal distribution of permeability ratio for models I, II, III and IV with experimental data [5] for *Pseudomonas aeruginosa* over the network of spheres.

reduction trend compared with the experimental results while Model I over predicts the reduction in permeability. It should be noted that other than this shift in the start of the reduction, the models prediction and experimental curves display a similar trend for permeability.

8. Conclusions

Biofilm formation has been investigated based on four models, which capture the main physical attributes of different pertinent works in the literature. The effect of different initial liquid porosities and thicknesses of the biofilm on the results are investigated. It is shown that initial conditions have a significant effect on the transient phase of the biofilm growth. Our results also indicate the advective flux of nutrients do not have a substantial effect on the biofilm growth. The obtained dynamic biofilm thickness from these models is applied to a network of spheres representing the porous medium, resulting in the porosity and permeability of the porous structure during the biofilm formation. The results from the biofilm models are compared with experimental data for a very common type of bacteria namely, *Pseudomonas aeruginosa*. The experimental data from Cunningham et al. [5] display a better qualitative agreement with our results. The models presented in this work properly account for both the macro- and micro-scales of the biofilm growth. These aspects are absent in prior models in this area.

References

[1] P.S. Stewart, A.K. Camper, S.D. Handran, C.T. Huang, M. Warnecke, Spatial distribution and coexistence of *Klebsiella pneumonia* and *Pseudomonas aeruginosa* in biofilms, Microb. Ecol. 33 (1997) 2–10.
[2] J. Wimpenny, Structural determinants in biofilm formation, Biofilms: Recent Advances in their Study and Control, Harwood Academic Publishers, Amsterdam, 2000. pp. 35–49.
[3] I.B. Beech, R.C. Tapper, R.J. Gubner, Microscopy methods for studying biofilms, Biofilms: Recent Advances in their Study and Control, Harwood Academic Publishers, Amsterdam, 2000. pp. 51–70.
[4] R.A. Calderone, Introduction and historical perspectives, Candida and Candidiasis, ASM Press, Washington, DC, 2002. pp. 3–13.
[5] A.B. Cunningham, W.G. Characklis, F. Abedeen, D. Crawford, Influence of biofilm accumulation on porous media hydrodynamics, Environ. Sci. Technol. (1991) 1305–1311.
[6] B.E. Rittmann, Where are we with biofilms now? Where are we going?, Water Sci Technol. 55 (8–9) (2007) 1–7.
[7] B.E. Rittmann, The significance of biofilm in porous media, Water Resour. Res. 29 (7) (1993) 2195–2202.
[8] W. Gujer, O. Wanner, Modeling mixed population biofilms, in: W.G. Characklis, K.C. Marshall (Eds.), Biofilms, Wiley, New York, 1990, pp. 397–443.

[9] H. Eberl, E. Morgenroth, D. Noguera, C. Piocioreanu, B. Rittmann, M. Van Loosdrecht, O. Wanner, Mathematical modeling of biofilms, IWA, 2006.
[10] E.B. Rittmann, P.L. McCarty, Model of steady-state-biofilm kinetics, Biotechnol. Bioeng. XXII (1980) 2343–2357.
[11] D. Gapes, J. Pérez, C. Picioreanu, M.V. Loosdrecht, Modeling biofilm and floc diffusion processes based on analytical solution of reaction–diffusion equations, Water Res. 40 (2006) 3144–3145.
[12] Sh. Qi, Morgenroth, Modeling steady-state biofilms with dual-substrate limitations, J. Environ. Eng. 131 (2005) 320–326.
[13] E.B. Rittmann, P.L. McCarty, Evaluation of steady-state-biofilm kinetics, Biotechnol. Bioeng. XXII (1980) 2359–2373.
[14] B.E. Rittmann, J. Manem, Development and experimental evaluation of steady-state, multispecies biofilm model, Biotechnol. Bioeng. 39 (1992) 914–933.
[15] M. Fouad, R. Bhargava, A simplified model for the steady-state biofilm activated sludge reactor, J. Environ. Manage. 74 (2005) 245–253.
[16] O. Wanner, W. Gujer, A multispecies biofilm model, Biotechnol. Bioeng. XXVIII (1986) 314–328.
[17] O. Wanner, A.B. Cunningham, R. Lundman, Modeling biofilm accumulation and mass transport in a porous medium under high substrate loading, Biotechnol. Bioeng. 47 (1995) 703–712.
[18] S. Taylor, P. Jaffe, Substrate and biomass transport in a porous medium, Water Resour. Res. 26 (9) (1990) 2181–2194.
[19] B. Chen, Numerical simulation of biofilm growth in porous media, J. Comput. Appl. Math. 103 (1999) 55–66.
[20] L.E. Allison, Effect of microorganisms on permeability of soil under prolonged submergence, Soil Sci. 63 (1947) 439–450.
[21] S.W. Taylor, P.C.D. Milly, P. Jaffe, Biofilm growth and the related changes in the physical properties of a porous medium 1-experimental investigation, Water Resour. Res. 26 (9) (1990) 2153–2159.
[22] S. Taylor, P.C.D. Milly, P. Jaffe, Biofilm growth and the related changes in the physical properties of a porous medium, 2. Permeability, Water Resour. Res. 26 (9) (1990) 2161–2169.
[23] S. Taylor, P.C.D. Milly, P. Jaffe, Biofilm growth and the related changes in the physical properties of a porous medium, 3. Dispersivity and model verification, Water Resour. Res. 26 (9) (1990) 2171–2180.
[24] R. Bakke, M.G. Trulear, W.G. Characklis, Activity of *Pseudomonas aeruginosa* in biofilms: steady state, Biotechnol. Bioeng. XXVI (1984) 1418–1424.
[25] M.A. Siebel, Binary population biofilms, Ph.D. diss., Montana State University, Bozeman, MT, 1987.
[26] J. Kozeny, Uber kapillare leitung des wassers im boden, Sitzungsber. Akad. Wiss. Wien. 136 (1927) 271–306.
[27] P.C. Carman, Fluid flow through a granular bed, Trans. Inst. Chem. Eng. Lond. 15 (1937) 150–156.
[28] J.W. Costerton, P.S. Stewart, E.P. Greenberg, Bacterial biofilms: a common cause of persistent infections, Science (1999) 1318–1322.
[29] J. Bear, Dynamics of Fluids in Porous Media, American Elsevier, New York, 1972.
[30] R.D. Cadle, Particle size theory and industrial applications, Reinhold Pub. Corp., New York, 1965.
[31] K. Khanafer, K. Vafai, The role of porous media in biomedical engineering as related to magnetic resonance imaging and drug delivery, Heat Mass Transfer 42 (2006) 939–953.
[32] B. Alazmi, K. Vafai, Analysis of variable porosity, thermal dispersion, and local thermal nonequilibrium on free surface flows through porous media, ASME J. Heat Transfer 126 (2004) 389–399.
[33] A. Khaled, K. Vafai, The role of porous media in modeling flow and heat transfer in biological tissues, Int. J. Heat Mass Transfer 46 (2003) 4989–5003.
[34] M.W. Lee, J.M. Park, One-dimensional mixed-culture biofilm model considering different space occupancies of particulate components, Water Res. 41 (2007) 4317–4328.
[35] O. Wanner, P. Reichert, Mathematical modeling of mixed-culture biofilms, Biotechnol. Bioeng. 49 (1996) 172–184.
[36] E. Alpkvist, C. Picioreanu, M.C.M. Van Loosdrecht, A. Heyden, Three dimensional biofilm model with individual cells and continuum EPS matrix, Biotechnol. Bioeng. 94 (5) (2006) 961–979.
[37] S.K. Tiwari, K.L. Bowers, Modeling biofilm growth for porous media applications, Math. Comput. Model. 33 (2001) 299–319.